RSC Advances

PAPER

View Article Online
View Journal | View Issue

Cite this: *RSC Adv.*, 2020, **10**, 37005

Effects of amino acids on conversion of calcium carbonate to hydroxyapatite

Sun Yanyan,[a] Wang Guangxin,[a]* Sun Guoqing,[b] Wang Yaming,[a] Li Wuhui[a] and Akiyoshi Osaka[ac]

Conversion of calcium carbonate (calcite; CC) to hydroxyapatite (HAp) was examined when the CC particles of sub μm size were soaked at 37 °C for up to 10 d in 0.15 M K_2HPO_4 (20 ml), whose pH was set to 3–12. Here, the solution contained amino acids, such as glutamine (Glu), arginine (Arg), and glycine (Gly), and their content varied from 0–1.0 g per ml of solution. From the X-ray diffraction (XRD) intensity of the 104 and 211 diffractions of calcite and apatite, respectively, it was seen that the presence of the amino acids promoted the conversion. This was supported by the thermogravimetry (TG) results. The highest promotion was observed at 0.5 g addition of amino acids to the phosphate solution, while Glu showed the highest promotion among the amino acids and Gly the lowest. A scanning electron microscopy study indicated that petal-like HAp nano-crystallites covered the entire surface of the CC particles when they were soaked in the phosphate solution with 0.1 g or more of amino acid for 10 d. The XRD intensity ratio 104(CC)/211(HAp) indicated greater CC to HAp conversion in the solutions at pH 3 and 6 than in the more alkaline solutions. This was attributed to the dissolution of CC in the acidic solutions, which was confirmed by bubbling in these solutions.

Received 6th September 2020
Accepted 30th September 2020

DOI: 10.1039/d0ra07636h

rsc.li/rsc-advances

1. Introduction

Hydroxyapatite (HAp, $Ca_{10}(PO_4)_6(OH)_2$) is the main inorganic component of human bones and teeth.[1,2] Because of its excellent biocompatibility, bone conductivity, bioactivity, safety and non-toxicity, it is widely used in the repair and regeneration of hard tissue defects, drug delivery and other fields.[3–6] For some implant materials, a good bioabsorbability is required. But HAp is the most resistant calcium phosphate to bioabsorbability.[7] In order to obtain a good bioabsorbability, calcium carbonate (CC) is introduced. CC is one of the most common minerals with a variety of sizes, and has been proved to be a good candidate for bone filling materials with good biodegradability and bone conductivity. CC can solve many problems of slow biodegradation of HAp based materials. CC can be directly or indirectly converted into HAp, and is thus a good precursor material for preparation of HAp. An implantation of CC in the body can help promote formation of new bones. Therefore, controlling the conversion of CC to HAp is of practical significance.[8–12]

An ideal bone repair material should mimic the natural bone matrix in terms of structure and composition to the greatest extent, and build an environment suitable for cell growth *in vitro*.[13] The human bone tissue is mainly composed of organic biomolecules and inorganic apatite. The organic biomolecules regulate the morphology and structure of inorganic apatite crystals. Therefore, it is of great significance to prepare bone repair materials with components and crystal structure similar to natural bone.[14,15] Because amino acid is a physiological substance of human body and can move freely in all tissues of human body through blood circulation, it is a natural choice to be used to regulate CC to HAp. Amino acid is also an effective regulator of HAp nucleation and growth, and can significantly affect the adsorption and release kinetics.[16–19] These cited studies found that an introduction of amino acids during synthesis of HAp changes the growth of initial crystalline domains along the *c*-axis and *a*-axis directions, thus changing morphology and dimensions of HAp particles.

In this study, the acidic amino acid L-glutamic acid (Glu), neutral amino acid L-glycine (Gly) and basic amino acid L-arginine (Arg) as typical amino acids with amino and carboxyl groups were used to study their effects on conversion of CC to HAp. The molecular structures of these 3 amino acids are shown in Scheme 1, and some of their physical properties are summarized in Table 1.[20] To our knowledge, it is rarely reported in literature that amino acids are used to control the conversion of CC to HAp. In addition, a simple solution immersion method was adopted to convert CC into hollow porous flower-like HAp, which was widely used in biomedical field because of its large specific surface area, high surface activity and strong adsorption capacity.[21–23]

[a]*Department of Materials Science and Engineering, Henan University of Science and Technology, Luoyang, Henan Province 471023, China. E-mail: wgx58@126.com*

[b]*School of Vehicle Engineering, Luoyang Institute of Technology, Luoyang, Henan Province 471023, China*

[c]*Faculty of Engineering, Okayama University, Tsushima, Okayama 700-8530, Japan*

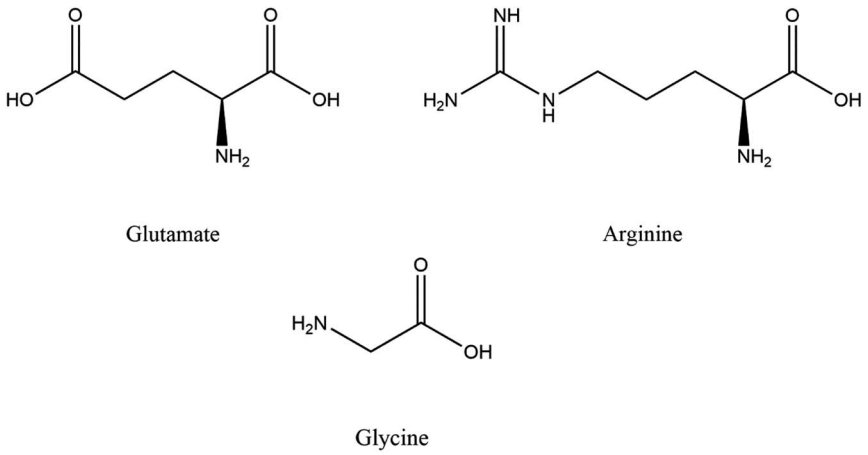

Scheme 1 Scheme of amino acids.

Table 1 pK_α values and isoelectric points (pI) of the amino acids used in this work; from Nelson and Cox[18]

Amino acid	Sample code	pK_α COOH	pK_α NH_2	pK_α side chain	pI
Glycine	Gly	2.34	9.6		5.97
Arginine	Arg	2.17	9.04	12.48 (guanidino)	10.76
Glutamate	Glu	2.19	9.67	4.25 (γ-COOH)	3.22

Therefore, this study also provides a new economic and convenient way of preparing hollow porous HAp.

2 Materials and experimental methods

Materials used in this study include sub-micrometer sizes or nanometer-sized CC particles supplied by Shiraishi Kogyo Kaisha (Osaka, Japan), and reagent grade chemicals supplied by Kaitong Chemical Reagent Corporation, Tianjin, China. Different masses (0.05, 0.1, 0.3 and 1 g) of the 3 amino acids (Gly, Arg and Glu) were dissolved in 0.15 M (M = mol L^{-1}) K_2HPO_4 solution. The pH value of solutions was initially adjusted to 3.0, 6.0, 7.0, 10.0 and 12.0 with 0.1 M HCl and KOH after adding amino acids. CC particles (0.5 g; 5 mmol) were dispersed into phosphate solutions (20 ml) with amino acids and held in 50 ml polystyrene bottles with tight caps. Note here that the solution pH 3 would increase due to the acid decomposition of CC to Ca^{2+} and CO_3^{2-} accompanying evolution of CO_2. The detailed pH increase was touched upon at the relevant text and figures below. An element ratio of Ca/P = 1.67 and a liquid-to-solid ratio of 0.5 g/20 ml were kept constant throughout this study. Bottles were kept still in an electric oven at 37 °C up to 10 days without stirring to simulate the biological environment of human body. After the soaking procedure, particles were gently rinsed with distilled water for at least three times. They were then placed in glass Petri dishes with a loose cover and dried in electric oven at 60 °C for 12 hours. Each experiment was repeated three times. A blank reaction without adding any amino acids was also performed as a control experiment.

Dry powders were sputter-coated with Au to observe their morphologies in SEM (JEOL JSM-7800F, Tokyo, Japan) operated at a 5 kV acceleration voltage. Crystal phases were identified with a XRD diffractometer (D8 ADVANCE, Cu Kα; λ = 0.1542 nm, Bruker, Berlin, Germany), where XRD profiles were taken at 8–70° in θ–2θ mode with a scanning step of 0.02° (2θ) and a holding time of 0.2 s. FTIR (IRTracer-100, Tokyo, Japan) and Raman (Invia, Renishaw, UK) spectroscopy were used to identify CC conversion products and evaluate their properties and chemical structures. FTIR was processed with KBr tablet with a spectral resolution of 4 cm^{-1}, and a scanning range of 4000–400 cm^{-1}. The laser wavelength of Raman spectrum is 532 nm. Thermal stability of conversion products was tested using TG (STA 449C, Germany) with a heating rate of 10 K min^{-1} from 25 °C to 800 °C in nitrogen.

3 Results and discussions

3.1 Effects of different amino acid contents on CC conversion

Fig. 1 shows XRD patterns of CC conversion products when the CC particles were soaked in 0.15 M K_2HPO_4 with pH 10 at 37 °C for 10 d. Here, "Con" stands for "control" representing the conversion product in the phosphate solution without any amino acid, while Gly, Arg, and Glu respectively represent the products in the solution containing each amino acid. This notation applies to other figures in the following. It can be seen from Fig. 1 that all XRD peaks before and after addition of the 3 amino acids are characteristie peaks of CC and HAp with slightly different intensities. Most peaks were indexed according to ICDD 86-0174 (calcite) and ICDD 09-0432 (HAp). It is found by comparison that HAp peaks appear in both (002) and (211) directions. The addition of amino acids significantly reduced the (104) peak intensity of CC, indicating that amino acids can speed up the CC conversion process. With increasing

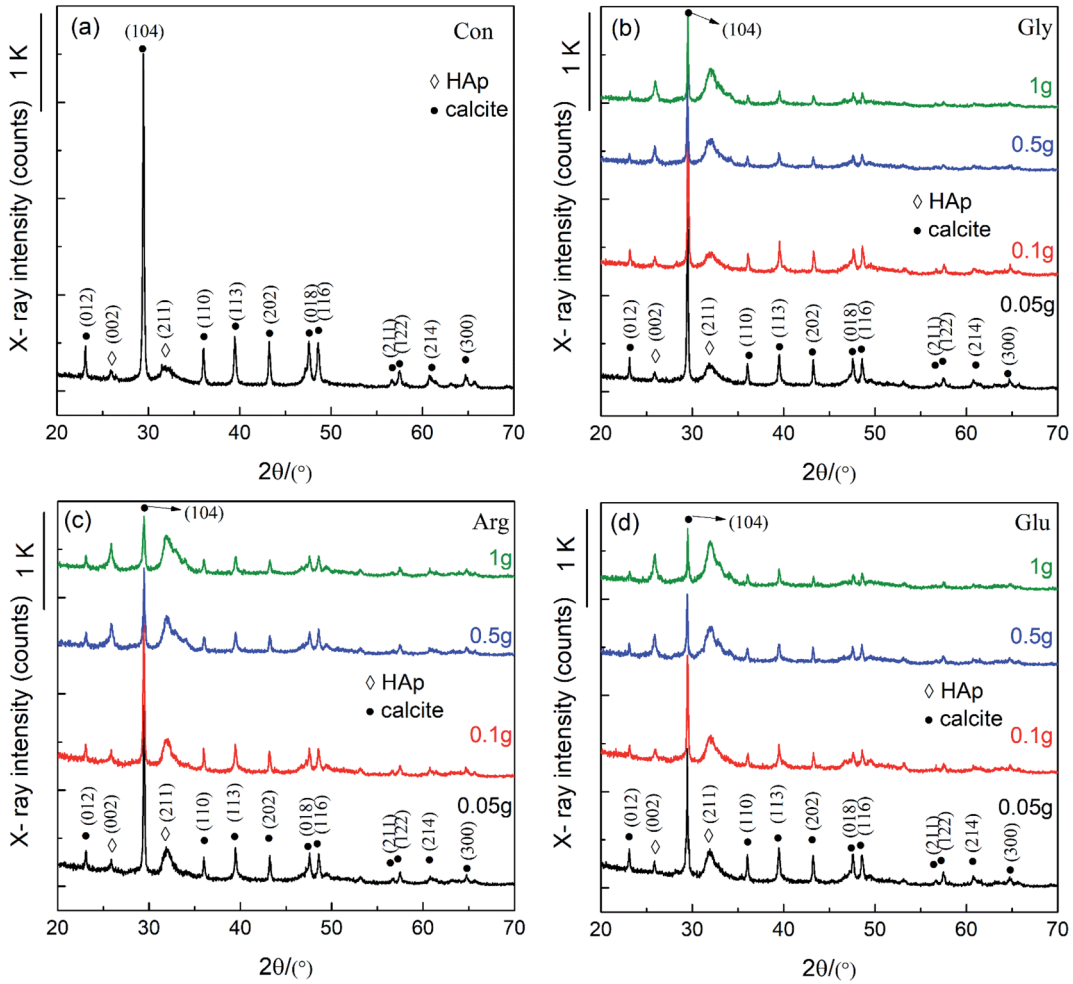

Fig. 1 XRD of the conversion products when CC (calcium carbonate) was soaked in 0.15 M K_2HPO_4 with pH 10 at 37 °C for 10 d. The amino acids content was none (a), while 0.05–1 g of Gly (b), Arg (c), and Glu (d).

amount of Glu, Arg and Gly, (211) peak intensity of HAp gradually increases, accompanying (112) and (300) peaks emerged in the 30–35° region, indicating that addition of Glu, Arg and Gly stimulated the formation of HAp. Glu and Arg have a stronger effect on the conversion of CC than Gly. This was explained in terms of the acid–base characteristics of each amino acid. Glu is an acidic amino acid, and its molecule is rich in carboxyl ($-COO^-$). Arg is a basic amino acid, and its molecule is rich in amino ($-NH_3^+$). Therefore, Glu and Arg molecules can specifically bind to Ca^{2+} and phosphate ions in solution to promote the conversion of CC and increase the crystalline core of HAp, thus more HAp can be converted from CC.[2,16,18] But Gly is a neutral amino acid and has no side groups, and its number of basic amino groups and acidic carboxyl groups in molecule are equal, therefore showing a non-polarity.

In order to further characterize chemical compositions of CC conversion products prepared with addition of different amino acids, FTIR and Raman spectra were carried out. Results are shown in Fig. 2. In Fig. 2a, the basic vibration peaks of phosphate before and after adding different amino acids appeared at 1038 cm^{-1} (ν_3), 966 cm^{-1} (ν_1), 604 cm^{-1} and 565 cm^{-1} (ν_4), 467 cm^{-1} (ν_2), respectively. Peaks at 3742 cm^{-1} and 669 cm^{-1} correspond to the stretching and bending vibrations of hydroxyl (OH^-) and are considered to be the characteristic peaks of HAp. In addition, peaks observed at 3420 cm^{-1} and 1646 cm^{-1} are due to the tensile and flexural vibrations of adsorbed water.[24] Peaks at 1429 cm^{-1}, 876 cm^{-1}, and 713 cm^{-1} are attributable to the antisymmetric expansion, out-of-plane bending, and in-plane bending of CO_3^{2-}.[25] It indicates that part of CO_3^{2-} may enter HAp lattice and replace part of OH or PO_4^{3-} to form A-type or B-type HAp. Comparing with the control group, one can see that the characteristic peak of phosphate increased and the characteristic peak of CO_3^{2-} decreased after addition of amino acids. This also indicates that addition of amino acids affects the conversion of CC to HAp.

Since no characteristic peaks of amino acids were detected in FTIR measurement, Raman spectrum detection was performed to make sure if amino acids adsorb on HAp surfaces. As shown in Fig. 2b, peaks at 424 cm^{-1} (ν_2), 585 cm^{-1} (ν_4), 963 cm^{-1} (ν_1), and 1060 cm^{-1} (ν_3) are the basic vibration peaks of phosphate. The characteristic peaks of CO_3^{2-} appeared at 713 cm^{-1} and 1437 cm^{-1}, and the characteristic peaks of adsorbed water

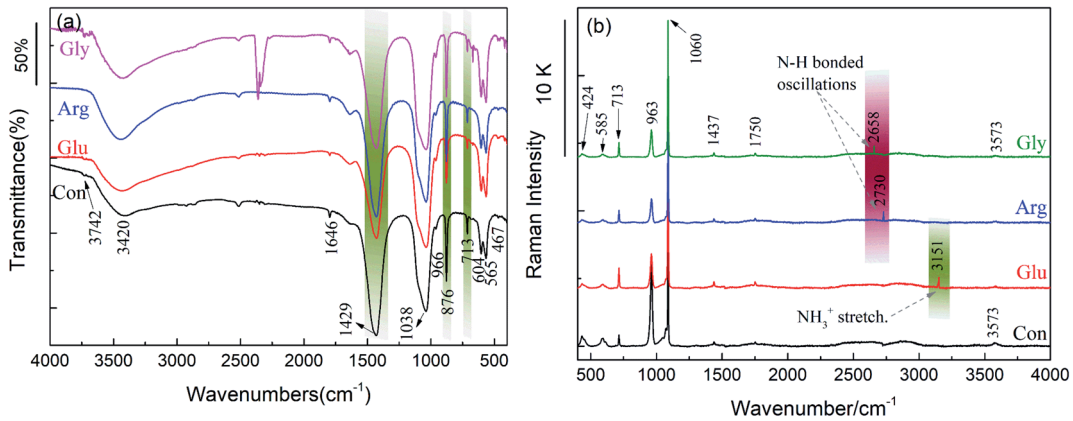

Fig. 2 FTIR spectrum (a) and Raman spectrum (b) of the conversion products with 0.1 g Gly, Arg and Glu respectively after soaked in 0.15 M K_2HPO_4 with pH 10 at 37 °C for 10 d.

appeared at 1750 cm^{-1}.[26] These results are consistent with the results of FTIR. But peaks not detected by FTIR were detected in Raman spectrum. The vibration peak of Gly at 2658 cm^{-1} and the vibration peak of Arg at 2730 cm^{-1} are both N–H bonding vibrations. The vibration peak of Glu at 3151 cm^{-1} is attributed to the stretching vibration of NH_3^+.[27] This indicates that a small part of amino acid molecules are adsorbed on surface of HAp and confirms that Raman spectrum is more sensitive to structures and therefore suitable for observing amorphous structures and phase transition of substances.

To evaluate the thermal stability of HAp at high temperatures, thermogravimetric (TG) analysis was conducted. Because amino acids adhering to sample surfaces may affect test results, samples were rinsed with distilled water at least three times before the TG tests. Fig. 3 shows TG curves of CC conversion products prepared with and without addition of different amino acids. These mass loss curves show several thermal transition stages in the testing temperature range. Initial mass losses at 25–280 °C are believed to be caused by the removal of chemically unbound water molecules and the decomposition of highly volatile impurities (for example, adsorbed carbon dioxide). Mass losses between 280 °C and 600 °C are mainly due to the loss of adsorbed water, chemically bound water and amino acid molecules. At higher temperatures (T > 600 °C), mass losses are due to the removal of carbonate ions embedded in HAp and unreacted CC. During the entire heating process, the control sample without amino acids lost 24.9% weight, while samples prepared with Glu, Gly and Arg lost 16.9%, 21.3% and 18.8% weights, respectively. The mass loss of the control sample is greater than samples prepared with addition of amino acids. The XRD profiles in Fig. 1 and 5 showed that the diffraction of CC was somehow dependent on the amino acid in the phosphate solutions. That is, the samples for the TG analysis were different in the residual amount of CC, and the samples had more CC would show more decrease in weight on the TG chart. The weight loss was due to the thermal decomposition of CC, and thus it depended upon the fraction of CC converted to HAp. The addition of amino acids promote the conversion of CC to HAp. And HAp is an inorganic phase with a good thermal stability and is not easy to decompose.[23] Another possibility is the residue of carbon, remained on the samples as a result of incomplete decomposition of the amino acids. Yet, this effect would be neglected because the samples were rinsed after the soaking experiments. The sample prepared with Glu shows the smallest mass loss, indicating that Glu has a stronger promoting effect on the conversion of CC to HAp. This agrees well with the XRD and FTIR results shown in Fig. 1 and 2.

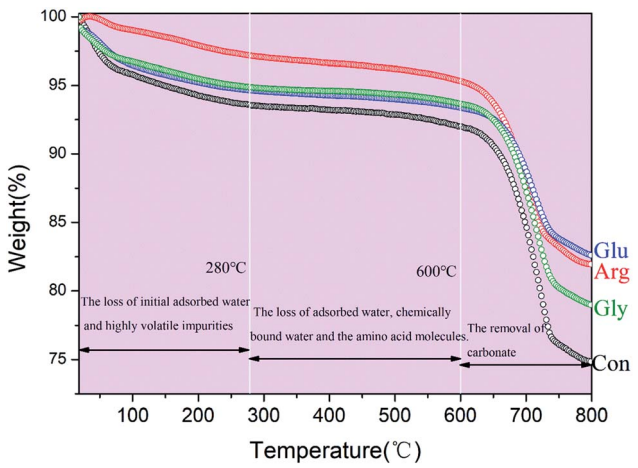

Fig. 3 TG profiles of the conversion products with 0.1 g Gly, Arg and Glu respectively after soaked in 0.15 M K_2HPO_4 with pH 10 at 37 °C for 10 d.

Fig. 4 shows SEM images of CC conversion products in the phoshate solutions of pH 10 with and without amino acids. Fig. 4a shows the morphology of the control sample prepared without adding amino acids. It can be seen from Fig. 4a that there are many unreacted CC particles, and some of them have been converted into petal-like porous HAp. Fig. 4(b1)–(d1) show morphologies of CC conversion products prepared with additions of 0.05, 0.1 and 1 g Gly, respectively. After adding 0.05 g Gly (Fig. 4(b1)), petal-like HAp is formed between CC particles. Although most of CC is converted into petal-like HAp, there are still some CC particles not completely converted. When 0.1 g Gly

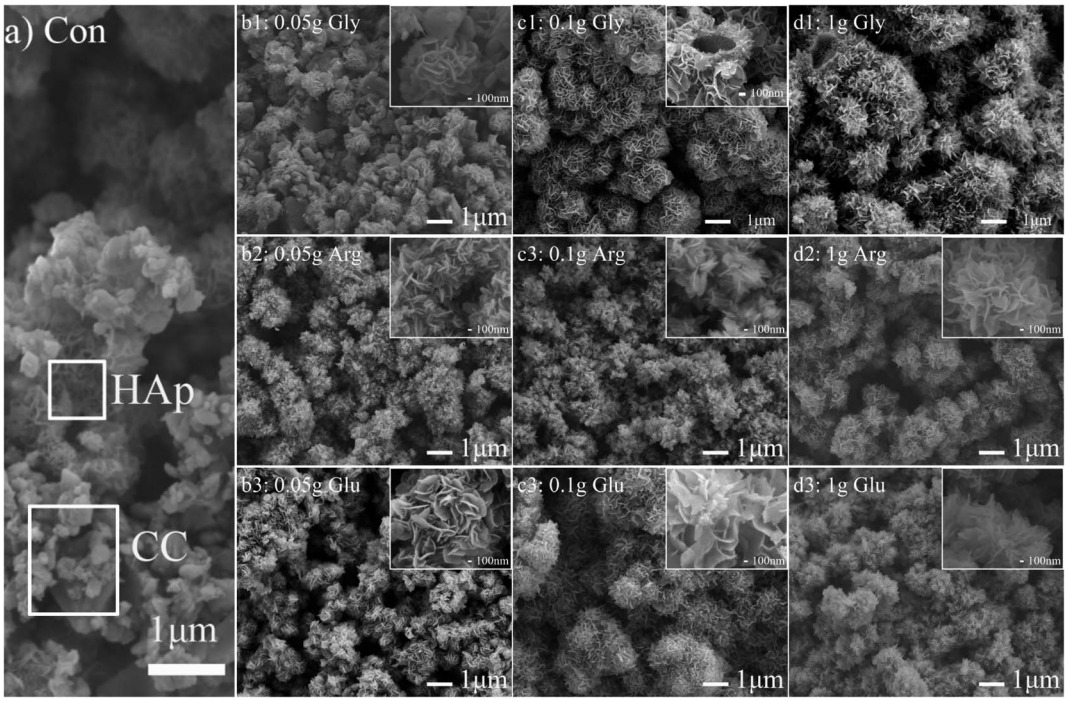

Fig. 4 SEM images of the conversion products without adding amino acids (a) and with adding different amounts (0.05 g, 0.1 g and 1 g) Gly, Arg and Glu respectively after soaked in 0.15 M K_2HPO_4 with pH 10 at 37 °C for 10 d. The inserts in the upper right corner are close-up images.

was added (Fig. 4(c1)), CC particles were converted into hollow spherical HAp aggregates with an average diameter of about 1.1 μm. Petal-like nanocrystals with a width of about 500 nm can be seen on surfaces of hollow spherical HAp aggregates. With an increase of Gly content to 1 g, hollow spherical HAp aggregates become bigger and they grow gradually together. The width of petal-like nanocrystals is reduced to about 200 nm. In short, the size of aggregates gradually increases, but the size of petal-like nanocrystals gradually decreases, with increasing Gly content. It is known that Gly is negatively charged in alkaline solution. This attracts Ca^{2+} and phosphate ions in solution and can thus change the surface polarity of HA.[2,28,29] With a small Gly content of 0.05 g, this effect is relatively small. But when the Gly content is large, more Gly molecules gather around CC particles, making local ion concentration oversaturated and leading to a formation of a large amount of crystal nuclei. As a result, large aggregates are formed.

Fig. 4(b2)–(d2) are morphologies of CC conversion products obtained by adding different amounts of Arg, whereas Fig. 4(b3)–(d3) show morphologies produced with different amounts of Glu. It can be seen that after adding 0.05 g Arg and Glu respectively, all CC surfaces are covered with a layer of HAp. And with an increase of Arg and Glu content, both sizes of petal-like nanocrystals and HAp aggregates increased slightly. In our experiment, pH of solution is less than the isoelectric point of Arg, so Arg is positively charged during the entire reaction process. It can adsorb negatively charged ions in solution, and may be adsorbed on negatively charged sites on HAp surface, so particle surface is also positively charged. That is, phosphate ions and protonated amino groups interact with Ca^{2+}, so that even a small Arg content can promote the conversion of CC to HAp. Glu is an acidic amino acid, which contains two carboxyl groups and one amino group. Depending on Glu concentration, the chelating ability of these groups with calcium ions and phosphate ions is different, and Glu is selectively adsorbed on specific crystal faces. Glu is negatively charged in alkaline solution, and the ionized carboxyl group adsorbs phosphate ions in solution and Ca^{2+} dissolved from CC, forming a large number of crystalline cores quickly.[2,29,30] As the reaction progresses, petal-like nanocrystals are gradually formed, which can promote the formation of HAp aggregates. This is in agreement with XRD results shown in Fig. 1.

3.2 Effects of pH values on CC conversion in presence of amino acids

Fig. 5 shows XRD profiles of conversion products prepared with 0.3 g Gly, 0.3 g Arg and 0.3 g Glu, and with varied solution pH 3–12 at 37 °C for 10 d. Note that the pH values appearing in the figures only indicate the initial ones before soaking the CC particles. Actually, pH of the phosphate solutions adjusted to 3 increased to 8–9 when the CC particles were soaked due to acid decomposition of CC to CO_3^{2-} and Ca^{2+}. For solution of initial pH 6 and 7, it reached pH 8–9 in final stage, respectively. Solutions of initial pH 10 and 12 showed a slight decrease of pH to ~10 and 11–12, respectively. It can be seen from Fig. 5 that with increasing pH value, the (104) peak intensity of CC shows a trend of first increasing and then decreasing, with the lowest (104) peak intensity being observed under acidic conditions. This shows that amino acids have the greatest impact on the conversion of CC under acidic conditions. The (012) peak

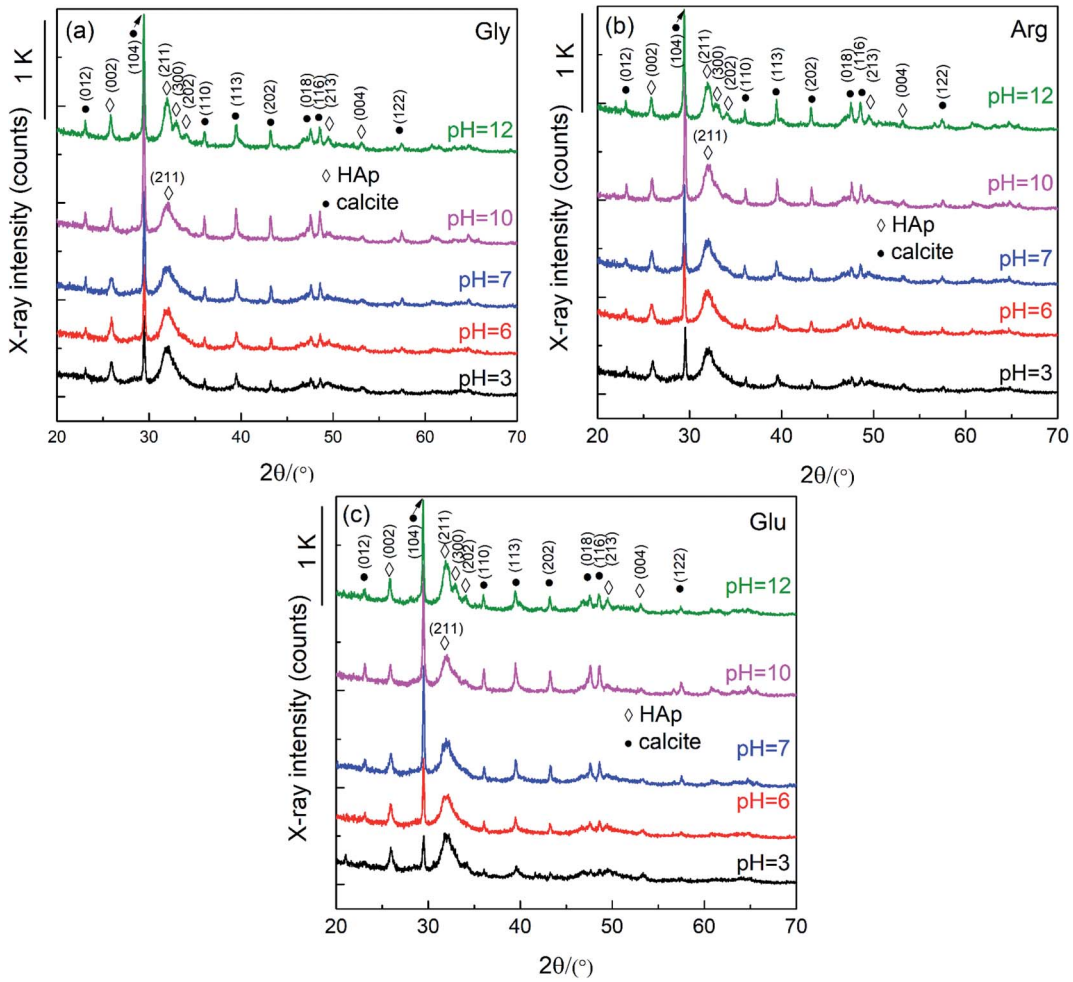

Fig. 5 XRD profiles of the conversion products with adding 0.3 g Gly (a), Arg (b) and Glu (c) respectively after soaked in 0.15 M K_2HPO_4 with varied pH 3–12 at 37 °C for 10 d. Note that the pH values appearing in the figures only indicate the initial ones before soaking the CC particles. The solution pH, originally adjusted at 3, increased to 8–9 due to acid decomposition of CC when the CC particles were soaked in the solution. For solution of initial pH 6, 7, 10 and 12, it reached pH 8–9, 8–9, 9–10 and 11–12 in final stage, respectively.

intensity of HAp increases gradually with increasing pH. At pH 12, (211), (300) and (202) peaks of HAp, located between 30° and 35°, are clearly separated, indicating that the crystallinity of HAp increases with the increase of pH.

An interesting observation is that solution of pH ≤ 7 generated some bubbles, with many being found on the container wall. This implies a CO_2 generation process. In our previous study we confirmed that under lower pH than 6 CC (calcite) particles were converted to DCPD or brushite, but not HAp. This difference is attributed to the amino acids to decrease the concentration of free calcium ion due to chelation. In addition, if CC particles are soaked in a pH 3 or 6 solution, they will dissolve in a solution that generates HCO_3 or CO_2 (formulas (1) and (2)). This is also the reason why the pH after the reaction increases and bubbles are generated during the reaction.

$$CaCO_3 + 2H^+ \text{ (pH 3 or 6 phosphate solution)} \rightarrow Ca^{2+} + 2HCO_3^- \quad (1)$$

$$CaCO_3 + 2H^+ \text{ (pH 3 or 6 phosphate solution)} \rightarrow Ca^{2+} + CO_2 + H_2O \quad (2)$$

Fig. 6 shows SEM images of the conversion products prepared with 0.3 g Gly, 0.3 g Arg and 0.3 g Glu, and with varied pH 3–12 at 37 °C for 10 d. It can be seen from Fig. 6 that CC particles are all converted into HAp aggregates which are assembled by petal-like nanocrystals. With increasing pH, the size of HAp aggregates gradually decreased, and the shape of HAp aggregates gradually changed from bayberry shape to ping-pong chrysanthemum shape, and finally to irregular shape. At the same time, petal-like nanocrystals gradually changed to needle-like ones. Comparing morphologies of samples prepared with addition of different amino acids, one can see that sizes of HAp aggregates increase in the order of Gly–Arg–Glu. This implies that the effect of promoting CC to HAp conversion increases in the order of Gly–Arg–Glu.

Fig. 7 shows a schematic illustration how amino acids (Gly, Arg and Glu) affect the conversion of CC to HAp. Amino acids can effectively control inorganic nucleation, crystallization,

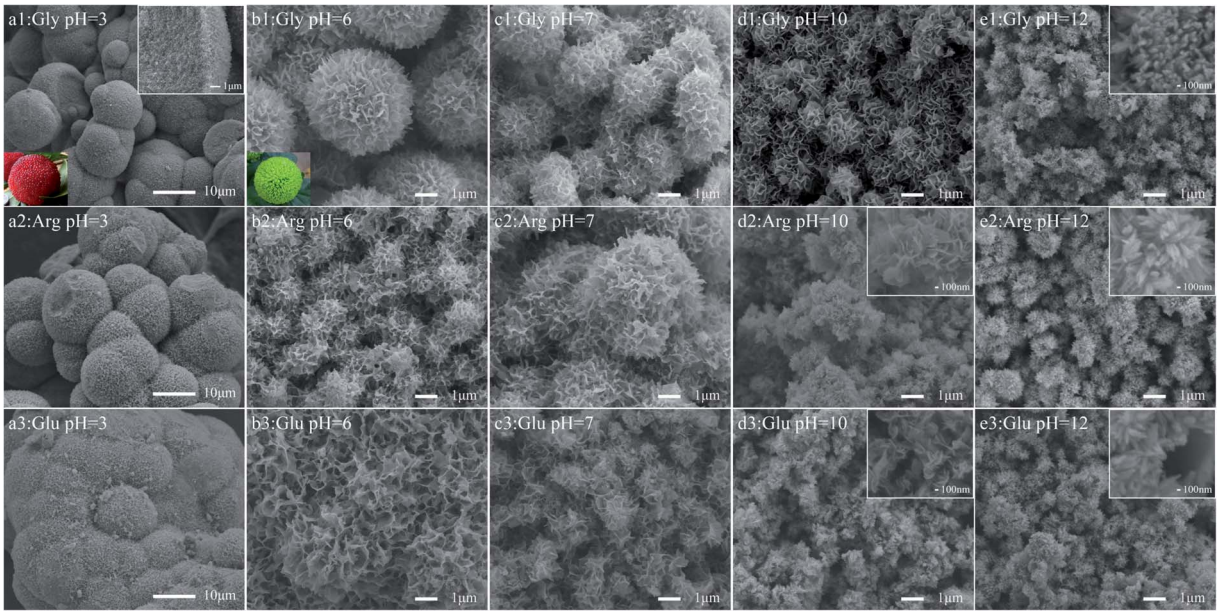

Fig. 6 SEM images of the conversion produces with 0.3 g Gly, Arg and Glu after soaked in 0.15 M K_2HPO_4 with varied pH 3–12 at 37 °C for 10 d. The inserts in the upper right corner of (a1), (e1), (d2), (e2), (d3) and (e3) are close-up images. The inserts in the lower left corner of (a1) and (b1) are photos of bayberry and ping pong chrysanthemum, respectively. Note that the pH values appearing in the figures only indicate the initial ones before soaking the CC particles.

growth and crystal transformation.[31] Different amino acids have different numbers of amino and carboxyl groups. Depending on their chain lengths, the stability of the complexes formed by amino acids with phosphate ions and calcium ions during the nucleation phase, and the ability of amino acids to adsorb on the surface of HAp crystals during the growth phase may be different.[32–34] At different pH, the conformational preference and spatial structure of amino acids may change, leading formation of different HAp morphologies with the same amino acid.[17] Gly, Arg and Glu have high affinities to surfaces of HAp, and have a strong ability to interact with calcium and phosphate ions. The interaction of HAp and amino acid are essentially electrostatic.[35]

An introduction of amino acid molecules can change the surface charge of HAp. The $-COO^-$, $-NH_3^+$ and side chain groups in amino acids play a great role in regulating the surface charge of HAp. The change of HAp surface charge will affect its protein adsorption capacity. The absorption sites mainly have surface Ca^{2+}, PO_4^{3-} or some small parts of –OH that may be exposed. Experiments show that this may be a complicated multi-site adsorption process, and sites can be "opened" or "closed" by changing the pH value.[36,37] If pH value of a solution is different, the influence of amino acids on CC conversion is different. When pH > 7 (and under alkaline conditions), CC is not easily decomposed in alkaline environment. Amino acid is positively charged during the whole reaction. Protonated ($-NH_3^+$), and $-NH_3^+$ amino groups will adsorb PO_4^{3-} in the solution to form a crystalline core, and then react with a small part of Ca^{2+} dissolved from CC in the solution to form a HAp crystalline core. They can also pass through the water molecule

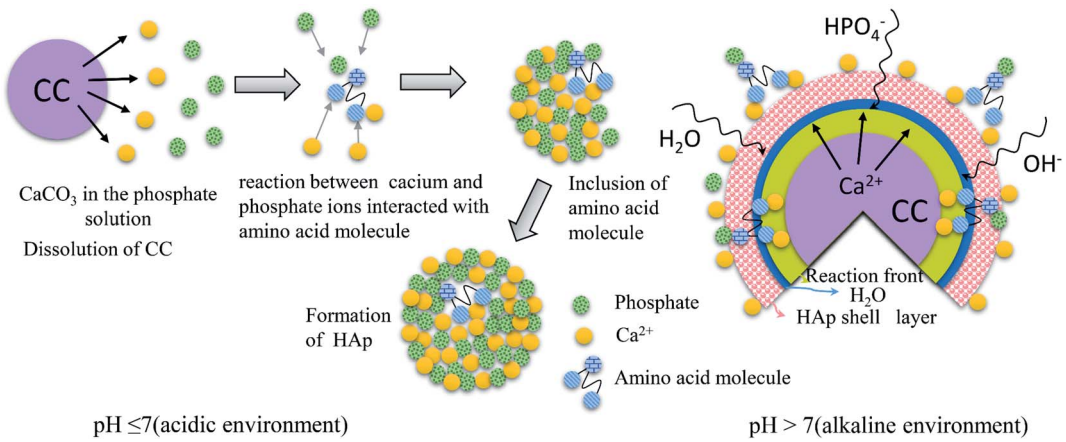

Fig. 7 Schematic illustration of amino acid affecting the conversion of CC to HAp.

channel in the HAp shell to reach the crystallization front and react with the decomposed Ca^{2+} inside the CC to form the HAp crystalline core, which can accelerate the conversion of CC (formula (3)). When pH < 7 (and under acidic conditions), CC is dissolved in acidic solution to release Ca^{2+}. Amino acids are negatively charged during the entire reaction. The carboxyl groups in amino acids are ionized ($-COO^-$), and $-COO^-$ will adsorb Ca^{2+} in the solution to form a large number of crystalline cores. Then it reacts with the phosphate ion and OH^- in the solution to form a charge-saturated area, which reduces the nuclear activation energy and accelerates the formation of HAp nuclei, thereby promoting the conversion of CC to HAp (formulas (1), (2) and (4)).

$$5CaCO_3 + 3HPO_4^{2-} + H_2O \rightarrow Ca_5(PO_4)_3(OH) + 5HCO_3^- + OH^- \quad (3)$$

$$5Ca^{2+} + 3HPO_4^{2-} + H_2O \rightarrow Ca_5(PO_4)_3(OH) + 4H^+ \quad (4)$$

4. Conclusion

The present study examined the effects of amino acids, such as Glu, Arg, and Gly, on the conversion of calcium carbonate (calcite; CC) to hydroxyapatite (HAp) when the CC particles were soaked at 37 °C up to 10 d in 20 ml 0.15 M K_2HPO_4 with or without those amino acid. Here, the weight/volume ratio was set to 0–1.0 g/20 ml and the solution pH was adjusted at 3–12.

(1) XRD profiles indicated that the presence of Glu, Arg, Gly in the phosphate solution promoted the CC-HAp conversion of CC to HAp. This was supported by the thermogravimetry. With increase in the amino acid content, the conversion was more promoted as well as the crystallinity of HAp was increased. A maximum promoting effect was observed when each amino acid was added by 0.5 g.

(2) The effects of promoting the conversion increased in the order: Gly < Arg < Glu.

(3) Scanning electron micrograph study showed that petal-like HAp nano-crystallites covered whole surface of the CC particles when the amino acid content exceeded 0.1 g.

(4) When soaked in the acidic phosphate solution (pH 3 and 6), greater CC conversion to HAp was observed than soaked in the solution with basic pH (7, or larger). This was attributed to the dissolution of CC under acid environment, confirmed by the CO_2 bubbling.

(5) When the phosphate solution increased basicity, the HAp aggregates shrunk in size, and their shape gradually changed from bayberry shape to ping-pong chrysanthemum shape, and finally they showed irregular shape. At the same time, the petal-like nanocrystals gradually changed to needle-like ones.

Conflicts of interest

☐ The authors declare that they have no known competing financial interests or personal relationships that could have appeared to influence the work reported in this paper.

☐ The authors declare the following financial interests/personal relationships which may be considered as potential competing interests:

The authors declare that they have no known competing financial interests or personal relationships that could have appeared to influence the work reported in this paper.

YY Sun *et al.*: Wang Guangxin
Henan University of Science and Technology
Luoyang, China

Acknowledgements

This work was supported by Chinese 02 Special Fund (Grand No. 2017ZX02408003), Innovative Research Team Program of Henan University of Science and Technology (Grant No. 2015XTD006), and Natural Science Fund Cultivation Project of Henan Province (Grant No. 162300410087).

References

1 Z. Chen, Y. Fu, Y. Cai, *et al.*, Effect of amino acids on the crystal growth of hydroxyapatite, *Mater. Lett.*, 2012, **68**, 361–363.
2 H. Pan, J. Tao, X. Xu, *et al.*, Adsorption processes of Gly and Glu amino acids on hydroxyapatite surfaces at the atomic level, *Langmuir*, 2007, **23**(17), 8972–8981.
3 L. F. Cóta, K. P. M. Licona, J. d. N. Lunz, *et al.*, Hydroxyapatite Nanoparticles: Synthesis by Sonochemical Method and Assessment of Processing Parameters *via* Experimental Design, *Mater. Sci. Forum*, 2016, **4101**, 896–901.
4 A. Anwar, Q. Kanwal, S. Akbar, *et al.*, Synthesis and characterization of pure and nanosized hydroxyapatite bioceramics, *Nanotechnol. Rev.*, 2017, **6**(2), 149–157.
5 X. Wu, X. Zhao, Yi Li, *et al.*, *In situ* synthesis carbonated hydroxyapatite layers on enamel slices with acidic amino acids by a novel two-step method, *Mater. Sci. Eng., C*, 2015, **54**, 150–157.
6 J. Kolmas, S. Krukowski, A. Laskus, *et al.*, Synthetic hydroxyapatite in pharmaceutical applications, *Ceram. Int.*, 2016, **42**(2), 2472–2487.
7 N. Yang, Q. Zhong, Y. Zhou, *et al.*, Controlled degradation pattern of hydroxyapatite/calcium carbonate composite microspheres, *Microsc. Res. Tech.*, 2016, **79**(6), 518–524.
8 K. Fu, Q. Xu, C. Jan, *et al.*, Characterization of a biodegradable coralline hydroxyapatite/calcium carbonate composite and its clinical implementation, *Biomed. Mater.*, 2013, **8**(6), 065007.
9 J. M. Li, D. P. Wei, Y. B. Hu, *et al.*, Synthesis of ultrafine green-emitting $BaCO_3$ nanowires with 18.5 nm-diameter by CO_2 vapor-assisted electrospinning, *Crystengcomm*, 2014, **16**(6), 964–968.
10 M. Takemaru, Y. Sakamoto, T. Sakamoto, *et al.*, Assessment of bioabsorbable hydroxyapatite for secondary bone grafting in unilateral alveolar cleft, *J. Plast. Reconstr. Aesthet. Surg.*, 2016, **69**(4), 493–496.

11 J. Li, Realizing single-crystalline vertically-oriented and high-density electrospun nanofibril bundles by controlled postcalcination, *CrystEngComm*, 2017, **19**(25), 3392–3397.
12 Y. Wang, Y. Xin Moo, C. Chen, *et al.*, Fast precipitation of uniform $CaCO_3$ nanospheres and their transformation to hollow hydroxyapatite nanospheres, *J. Colloid Interface Sci.*, 2010, **352**(2), 393–400.
13 S. Wang, Z. Zhao, Y. Yang, *et al.*, A high-strength mineralized collagen bone scaffold for large-sized cranial bone defect repair in sheep, *Regener. Biomater.*, 2018, **5**(5), 283–292.
14 G. Wei and P. X. Ma, Structure and properties of nano-hydroxyapatite/polymer composite scaffolds for bone tissue engineering, *Biomaterials*, 2004, **25**(19), 4749–4757.
15 A.-M. Yousefi, H. Oudadesse, R. Akbarzadeh, *et al.*, Physical and biological characteristics of nanohydroxyapatite and bioactive glassesused for bone tissue engineering, *Nanotechnol. Rev.*, 2014, **3**(6), 527–552.
16 S. Jack Kevin, G. Vizcarra Timothy and T. Matt, Characterization and surface properties of amino-acid-modified carbonate-containing hydroxyapatite particles, *Langmuir*, 2007, **23**(24), 12233–12242.
17 R. Sharma, R. R. Pandey, A. A. Gupta, *et al.*, *In situ* amino acid functionalization and microstructure formation of hydroxyapatite nanoparticles synthesized at different pH by precipitation route, *Mater. Chem. Phys.*, 2012, **133**(2–3), 718–725.
18 Z. Zhao, W. Shan, Y. Zhang, *et al.*, Fabrication and properties of degradable poly(amino acid)/nano hydroxyapatite bioactive composite, *J. Appl. Polym. Sci.*, 2012, **125**(4), 2502–2509.
19 W. -H. Lee, C. -Y. Loo, W. Chrzanowski, *et al.*, Osteoblast response to the surface of amino acid-functionalized hydroxyapatite, *J. Biomed. Mater. Res., Part A*, 2015, **103**(6), 2150–2160.
20 D. L. Nelson and M. M. Cox, *Lehninger principles of biochemistry*, 3rd edn, Worth Publishers, New York, 2000.
21 X. Xia, J. Chen, J. Shen, *et al.*, Synthesis of hollow structural hydroxyapatite with different morphologies using calcium carbonate as hard template, *Adv. Powder Technol.*, 2018, **29**(7), 1562–1570.
22 L. Wen, C. Chen, X. Ren, *et al.*, Hydrothermal fabrication of porous hollow hydroxyapatite microspheres for a drug delivery system, *Mater. Sci. Eng., C*, 2016, **62**, 166–172.
23 D. Gopi, J. Indira, L. Kavitha, *et al.*, Synthesis of hydroxyapatite nanoparticles by a novel ultrasonic assisted with mixed hollow sphere template method, *Spectrochim. Acta, Part A*, 2012, **93**, 131–134.
24 A. Kaflak, A. Ślósarczyk and W. Kolodziejski, A comparative study of carbonate bands from nanocrystalline carbonated hydroxyapatites using FT-IR spectroscopy in the transmission and photoacoustic modes, *J. Mol. Struct.*, 2011, **997**(1), 7–14.
25 A. Kaflak and W. Kolodziejski, Complementary information on water and hydroxyl groups in nanocrystalline carbonated hydroxyapatites from TGA, NMR and IR measurements, *J. Mol. Struct.*, 2011, **990**(1), 263–270.
26 P. E. Timchenko, E. V. Timchenko, E. V. Pisareva, *et al.*, Spectral analysis of allogeneic hydroxyapatite powders, *J. Phys.: Conf. Ser.*, 2017, **784**(1), 012060.
27 K. Balasubramanian, R. S. Krishnan and Y. Iitaka, Raman Spectrum of γ-Glycine, *Bull. Chem. Soc. Jpn.*, 1962, **35**(8), 1303–1305.
28 S. Krukowski, N. Lysenko and W. Kolodziejski, Synthesis and characterization of nanocrystalline composites containing calcium hydroxyapatite and glycine, *J. Solid State Chem.*, 2018, **264**, 59–67.
29 H. Pan, J. Tao, X. Xu, *et al.*, Adsorption processes of Gly and Glu amino acids on hydroxyapatite surfaces at the atomic level, *Langmuir*, 2007, **23**(17), 8972–8981.
30 W. T. Tsai Tim, W.-Ya Chen, Y.-H. Tseng, *et al.*, Phase transformation of calcium phosphates in the presence of glutamic acid, *Can. J. Chem.*, 2011, **89**(7), 885–891.
31 J. M. Tavafoghi, G. Yao and M. Cerruti, The importance of amino acid interactions in the crystallization of hydroxyapatite, *J. R. Soc., Interface*, 2013, **10**(80), 20120906.
32 S. Jack Kevin, G. Vizcarra Timothy and T. Matt, Characterization and surface properties of amino-acid-modified carbonate-containing hydroxyapatite particles, *Langmuir*, 2007, **23**(24), 12233–12242.
33 S. Koutsopoulos and E. Dalas, The effect of acidic amino acids on hydroxyapatite crystallization, *J. Cryst. Growth*, 2000, **217**(4), 410–415.
34 T. Matsumoto, M. Okazaki, M. Inoue, *et al.*, Crystallinity and solubility characteristics of hydroxyapatite adsorbed amino acid, *Biomaterials*, 2002, **23**(10), 2241–2247.
35 A. El Rhilassi, M. Mourabet, M. Bennani-Ziatni, *et al.*, Interaction of some essential amino acids with synthesized poorly crystalline hydroxyapatite, *J. Saudi Chem. Soc.*, 2016, **20**, S632–S640.
36 M. Tavafoghi Jahromi and M. Cerruti, Amino Acid/Ion Aggregate Formation and Their Role in Hydroxyapatite Precipitation, *Cryst. Growth Des.*, 2015, **15**(3), 1096–1104.
37 B. Palazzo, D. Walsh, M. Iafisco, *et al.*, Amino acid synergetic effect on structure, morphology and surface properties of biomimetic apatite nanocrystals, *Acta Biomater.*, 2008, **5**(4), 1241–1252.